

Thermal damping of quantum interference patterns of surface-state electrons

O. Jeandupeux, L. Bürgi, A. Hirstein, and H. Brune

Institut de Physique Expérimentale, Ecole Polytechnique Fédérale de Lausanne, CH-1015 Lausanne, Switzerland

K. Kern

*Institute de Physique Expérimentale, Ecole Polytechnique Fédérale de Lausanne, CH-1015 Lausanne, Switzerland
and Max-Planck-Institut für Festkörperforschung, Heisenbergstrasse 1, D-70569 Stuttgart, Germany*

(Received 16 December 1998)

The temperature-dependent damping of quantum-mechanical interference patterns from surface-state electrons scattering off steps on Ag(111) and Cu(111) has been studied using scanning tunneling microscopy (STM) and spectroscopy in the temperature range 3.5–178 K. The thermal damping of the electron standing waves is described quantitatively within a simple plane-wave model accounting for thermal broadening due to the broadening of the Fermi-Dirac distributions of sample and tip, for beating effects between electrons with different \mathbf{k}_{\parallel} vectors, and for inelastic collisions of the electrons, e.g., with phonons. Our measurements reveal that Fermi-Dirac broadening fully explains the observed damping for Ag and Cu. From the analysis of our data, lower limits of the phase-relaxation lengths at the Fermi energy E_F of the two-dimensional electron gas of $L_{\phi}(E_F) \geq 600$ Å at 3.5 K and ≥ 250 Å at 77 K for Ag(111), and of $L_{\phi}(E_F) \geq 660$ Å at 77 K and ≥ 160 Å at 178 K for Cu(111) are deduced. In contrast to integral measurements such as photoemission we measure L_{ϕ} close to E_F and also locally. The latter eliminates residual line widths due to surface defect scattering found in the integrating techniques. Our STM results, therefore, currently provide a very good absolute estimate of L_{ϕ} and the inelastic lifetime $\tau = L_{\phi}/v_F$, respectively. Our values can be combined with photoemission results on dL_{ϕ}/dT to derive the inelastic lifetime of surface state electrons at any T . [S0163-1829(99)02524-2]

I. INTRODUCTION

Shockley type surface states exist in the Γ -L-projected bulk band gap of the (111) surfaces of noble metals. These states have been intensively investigated by means of photoelectron spectroscopy.^{1–3} They form a two-dimensional (2D) nearly free-electron gas which is subjected to scattering at surface imperfections such as steps and point defects leading to periodic spatial oscillations of the electronic local density of states (LDOS). The standing LDOS waves are the analog to the well-known Friedel oscillations of the total charge density.⁴ The LDOS oscillations at surfaces can be understood as the interference of an electron wave traveling toward the scattering defect with the backscattered wave. The resulting quantum-mechanical interference patterns can be spatially resolved in scanning tunneling microscopy/spectroscopy (STM/STS).^{5–7} STM acquires a quantity roughly proportional to the surface LDOS in spectroscopic $dI/dV(E, x, y)|_z$ maps,⁸ whereas it displays the integral of the LDOS from E_F to $(E_F + eV)$ in conventional $z(x, y)|_{I, V}$ topographs. Standing electron waves have been reported in both imaging modes. These STM images of the spatial distribution of the LDOS around defects enabled an unprecedented direct access to several surface electronic properties. The dispersion relation $E(k)$ of the 2D electron gas has been determined by means of STM,^{5,6,9} with an accuracy comparable to state-of-the-art angle-resolved photoelectron spectroscopy (ARPES) studies.^{3,10} The advantage of STM in measuring the dispersion relation is the access to electronic states below and above E_F . Mapping of the 2D Fermi contour of surface states was achieved through the Fourier transform of STM topographs taken at very low bias voltage.¹¹

Finally, stationary solutions of the Schrödinger equation in two dimensions were visualized for particular geometries of the scattering potential.^{7,12–15}

A prerequisite for standing waves to appear is a sufficiently long phase coherence length L_{ϕ} , the mean length an electron travels without losing its phase memory. Several STM studies of standing waves point out the lack of knowledge about the phase coherence length of the 2D electrons. Also, the mechanisms underlying the decay of interference patterns observed at elevated temperatures have not yet been clarified. The former absence of measurements reporting standing waves on Cu(111) at 300 K was speculatively attributed to inelastic scattering,⁵ whereas thermal broadening of the Fermi-Dirac distributions was invoked for room-temperature measurements on Au(111).^{6,16} The goal of the present paper is to shed some light on the subject of coherence of 2D electrons as seen by STM/STS, and to derive experimental estimates on $L_{\phi}(T)$. We quantify the role of the various contributions—inelastic scattering, Fermi-Dirac broadening and beating—the latter two adding up to an apparent coherence loss. We present measurements of the temperature-dependent decay of standing waves on the (111) surfaces of Ag and Cu, from which we derive absolute estimates of L_{ϕ} at various temperatures.

The most intriguing contributions to the apparent coherence loss are inelastic scattering events, and the question arises of whether STM can furnish quantitative information on inelastic scattering of 2D electrons. Collisions of an electron with static scatterers like steps or adsorbates do not influence the phase coherence.¹⁷ In conducting systems, L_{ϕ} is reduced by inelastic scattering processes like electron-electron interaction at an appreciable electron energy, or by

electron-phonon interaction at higher temperatures. In semiconductors or thin metal films $L_\phi(E_F)$ is usually obtained indirectly by weak localization experiments.^{18,19} In inhomogeneous gold films $L_\phi(E_F)$ is of the order of some 10 nm at 20 K, and decreases as $1/T$ at higher T , whereas $L_\phi(E_F) \approx 100$ nm at 5 K in a 2D electron gas of GaAs/Al_xGa_{1-x}As heterostructures.^{18,19} A source of L_ϕ other than transport measurements has recently become available by high-resolution ARPES, revealing Lorentzian line shapes.^{10,20–22} The full peak width at half maximum Γ gives access to the lifetime τ via $\Gamma = \hbar/\tau$ and to the phase-coherence length $L_\phi = \tau v$, where v is the group velocity of the electrons. In contrast to ARPES, STM offers the possibility to determine locally the phase-relaxation length L_ϕ of surface-state electrons by analyzing the damping of the LDOS oscillations. Below we derive first absolute estimates of $L_\phi(E_F, T)$ for the Shockley-type surface states of Ag(111) and Cu(111). Since we perform our measurements near E_F and at surface spots that are bare of any defect, there is no observable residual inverse lifetime $1/\tau$ at 4 K.

The paper is organized as follows. After an experimental section we determine the dispersion relation of the Ag(111) surface state by measuring the wavelength of the LDOS oscillations as a function of energy. To analyze our STM data, in Sec. III B we introduce an analytic plane-wave model yielding $z(x)|_{I,V}$ for scattering at a straight step that extends infinitely in the y direction, with x being perpendicular to the step. The model accounts for (i) the decay caused by Fermi-Dirac broadening due to the finite temperature of the tip and sample, (ii) the beating appearing through the contribution of states with different \mathbf{k} vectors due to the finite bias voltage V , and (iii) the decay by phase-coherence loss due to inelastic scattering processes, e.g., with phonons. The only input for the model is the effective mass m^* and the band-edge energy E_0 , both quantities known from the dispersion relation. The performance of our model is demonstrated for high-resolution line scans taken at large tunneling voltages, thus showing pronounced beating effects. In Sec. III C the model is applied to analyze the temperature-dependent damping of the interference patterns near a monoatomic step on Ag(111). We obtain a lower limit for the phase-relaxation length of the surface electron gas L_ϕ at the various temperatures. In Sec. III D we present measurements for the temperature-dependent spatial damping of standing waves of the $\bar{\Gamma}$ surface state of Cu(111). Section III E discusses our STM results in comparison with results obtained from the investigation of line shapes in high-resolution photoemission.

II. EXPERIMENT

The measurements presented in this paper were acquired with a custom-built 4 K–5 T STM operating in UHV which we briefly describe here. The UHV chamber (see Fig. 1) is designed such that samples can be prepared in the sample holder under temperature control down to 40 K, enabling the self-assembly of low-dimensional structures via kinetically controlled growth.²³ The single crystal samples are hat shaped, and clamped on their brim into a sandwich Mo sample manipulator. Two sapphire spacers between Mo and crystal provide the electrical insulation necessary to apply

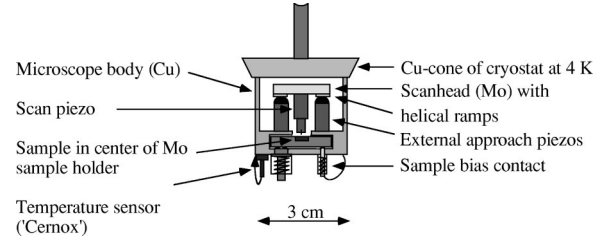


FIG. 1. Sketch of the UHV chamber and the 4 K–5 T scanning tunneling microscope.

the bias voltage V to the sample in the STM. The sapphire is also thermally insulating at high T , enabling fast and clean flashes for sample preparation. At low T the thermal conductivity of sapphire (along the c axis) reaches that of clean Cu, thus providing efficient sample cooling as well. The sample holder further has chromel/constantan thermocouple contacts, with their spring-loaded counterparts in the sample manipulator. Precise temperature measurement is achieved by contacting the thermocouple wires to different sides of the single crystal, ensuring that the thermocouple hot junction is located at the crystal.

After preparation of the substrate, and growth of the desired surface structures, the sample holder is transferred into the microscope with a wobble stick. We were seeking for isothermal sample transfer in order to preserve metastable growth structures. To achieve this we isolated the parts that are in touch with the sample holder (two CuBe-bars and a central steel-bayonet joint, together building a fork) by Teflon spacers from the wobble stick housing. Their thermal mass is small compared to the sample holder, and thus the temperature rise while transferring cold samples to the STM is minimized (the CuBe fork can additionally be pre-cooled for this purpose). Up to three samples can be held in UHV in a storage system which is also served by the wobble stick. New samples can be introduced into the UHV system through a load lock.

The STM is located in the center of a superconducting split pair magnet operating at 4.2 K, and providing magnetic fields of up to 5 T perpendicular to the sample surface. The split coil geometry of the magnet allows access to the STM via four bores ($\Phi = 50$ mm) arranged horizontally at 90° to each other. Sample transfer is performed through one of the bores while a second bore is used to watch the transfer from the side with a CCD camera. The other two bores are foreseen to dose small metal coverages onto the sample when placed in the STM, and for access with a laser, respectively. Thermal contact of the sample to the microscope body is achieved by sliding the sample holder into a drawer, with spring-loaded teflon cones firmly pressing it toward the top against a polished Cu surface (Fig. 1). Accordingly, the temperature of the STM and sample are at 4.9 K, close to that of liquid He. The coarse tip approach is achieved with the inertial rotation²⁴ of a Mo disk residing on three ruby balls glued to three piezo feet ($\Phi = 6.65$ mm) pointing to the top. The Mo disk provides helical ramps with a height difference of 0.5 mm. The disk carries in its center the central scan piezo, which itself carries the tip within a tube. Thus the beetle design²⁵ has been split (see Fig. 1) to provide good thermal contact to the sample while maintaining the convenient coarse approach and lateral displacement accomplished

by the inertial motion of the Mo disk on the ruby balls. To achieve reliable operation of the sliding motion down to 4 K, the surface of the Mo ramps was carefully polished. The microscope body itself is thermally and mechanically coupled to the cryostat by a copper cone-shaped disk which is firmly pressed by springs in the transfer rod against its counterpart located in the cryostat. We employed In to improve the thermal contact at the cone. The He bath cryostat together with the magnet were designed by Oxford Instruments. The cryostat is mounted on a CF-300 flange, and contains 42l He. A 30l liquid N₂ bath shields against room-temperature radiation.

Despite the advantage of having good thermal contact to the He bath, our choice to mount the STM rigidly to the cryostat implies rather careful vibrational damping. The low-frequency vibrations of the building (10–40 Hz) are efficiently damped by arranging three harmonic oscillators in a series. The first consists of a spring suspension of the base plate from the ceiling. The second harmonic oscillator is realized by a set of four commercial pneumatic damping elements (Newport) suspending the UHV chamber with respect to the base plate. The last damping stage is a set of three such elements supporting the cryostat with respect to the chamber. There is a CF-300 bellows (38 membranes) between the cryostat and the chamber. The lowest eigenfrequency of the overall suspension is $f_0 \approx 0.3$ Hz. For frequencies far above f_0 the transmission functions of the single harmonic oscillators can be multiplied with each other to obtain the overall transmission function. The transmission of external building vibrations to the cryostat is thus estimated to be $\ll 10^{-3}$ for all frequencies above 3 Hz. High-frequency vibrations, as acoustic noise, are efficiently damped by encapsulation of the UHV system into a soundproof cubicle. The measurements are performed while turning off all mechanical pumps and every power supply that has a fan. The power supply of the ion pump and the STM electronics (SPM 2000, RHK-technology TM) are situated outside the cubicle. Bubbling of liquid nitrogen in the shield is avoided by solidification with a rotary pump located in the basement of the building.

For the measurements presented in this paper, temperature variations in the microscope are simply achieved by removing liquid helium from the cryostat, giving rise to a temperature increase of the microscope over days, thus enabling drift-free STM measurements at well defined temperatures up to 300 K. The minimum temperature of 3.5 K was attained by pumping the liquid-He reservoir in the cryostat. At 4.9 K, the lateral drift of our STM is approximately 2 Å/h, and the stability along the z direction is of the order of 5/1000 Å. Thus atomic resolution is routinely obtained and, more demanding, quantum interference patterns of scattered surface-state electrons are readily resolved in $z(x,y)|_{I,V}$ topographs (see Fig. 2). The vertical stability is also crucial for the resolution achievable in dI/dV spectra recorded with open feedback loop. Furthermore the stability is not at all influenced by the presence of the magnetic field, and it is possible to record STM data on the very same surface spot at different values of the magnetic field.

The Ag(111) and Cu(111) surfaces have been cleaned by sequential cycles of Ar⁺ sputtering at 300 K and subsequent annealing to $T=870$ and 820 K, respectively. After this procedure, the surfaces had terraces of more than 2000 Å width

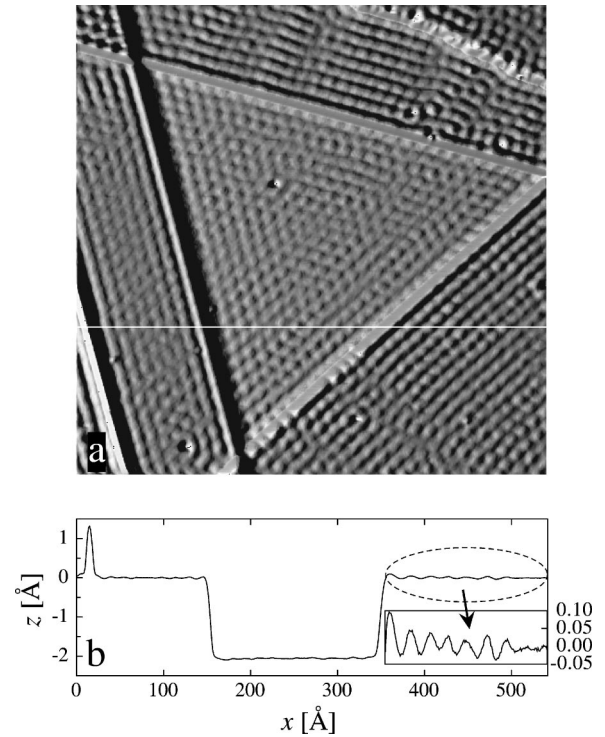


FIG. 2. (a) Constant-current STM topograph showing quantum interference of surface state electrons on a Cu(111) surface (raw data). The step structure was created by indenting the tip at a place nearby. The image area of 545×545 Å² exhibits three terrace levels and an atomic chain on the lower left-hand side [see also line scan (b) taken along the white line in (a)]. The gray levels correspond to illumination of the surface from the left-hand side. The image was acquired at $V=1.0$ mV and thus approximately shows the LDOS(x,y) at $E_F(I=1.1$ nA).

with a surface coverage of $\approx 0.02\%$ of a monolayer of impurities of unknown chemical identity. In our STM measurements the bias voltage V is applied to the sample. The electrochemically etched W tip was prepared by field emission and by controlled indentations into the surface. The conductance spectra $dI/dV(E)$ were measured under open feedback-loop conditions by conventional lock-in technique with a 1.2 kHz modulation of the bias voltage by about 5 mV rms.

III. RESULTS AND DISCUSSION

A. Dispersion relation of the Ag(111) surface state

In order to measure the dispersion relation of a surface state with STS, it suffices to take a single line scan perpendicular to a straight substrate step, and to measure a conductance map $dI/dV(x,E)$, while moving the STM tip on this line scan. Technically, the conductance map is acquired by taking $dI/dV(E)|_x$ spectra at every fourth topographic pixel x of the line scan while keeping the tip at a fixed height (open feedback condition). To avoid convolution between standing waves in the tip height z of the constant-current line scan and those in the dI/dV spectra,⁹ z is controlled at a large positive-bias voltage. Under these conditions, the current I contains contributions from electronic states with many different oscillation periods (k_{\parallel} values), which mini-

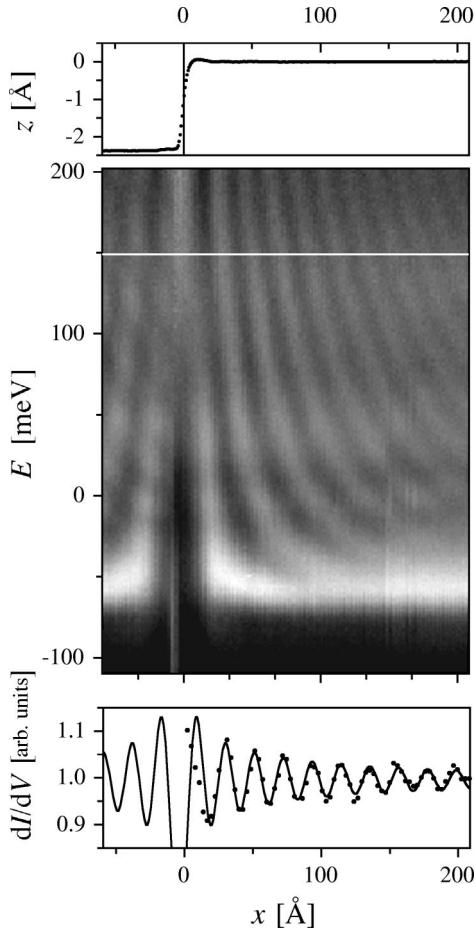


FIG. 3. Plot of the differential conductance dI/dV of Ag(111) at 5 K as a function of the lateral distance from the step x and of bias energy $E=eV$ with respect to E_F . The upper graph shows the constant-current line scan ($V=0.3$ V, $I=2.0$ nA) on which the STM tip was moved while taking the $dI/dV(V)$ spectra (peak-to-peak modulation of $\Delta V=10$ mV). The lower graph is a cut of the dI/dV plot taken along the white line at $E=148$ meV (dots), and the line is a fit by Eq. (1).

mizes the standing waves in the z signal. That way the tip is moved to a good approximation parallel to the plane defined by the atomic nuclei, unaffected by interference patterns in the LDOS. The differential conductance is then roughly proportional to ρ_{2D} , the 2D LDOS of the sample.^{8,9}

The result of such a measurement is shown for Ag(111) in Fig. 3. The upper graph displays the constant-current line scan on which the tip was moved while taking the $dI/dV(E)|_x$ spectra. As can be seen, at the bias voltage of $V=0.3$ V the tip-surface distance is almost uninfluenced by standing waves (only in the immediate vicinity of the step), and the tip closely follows the real topography. The $dI/dV(x,E)$ data are represented by gray levels as a function of the distance from the step edge x in abscissa and energy E in ordinate. The density plot in Fig. 3 nicely illustrates the dispersion of the Ag(111) surface state. From top to bottom the wavelength of the standing waves in the LDOS increases for energies approaching E_F , until it diverges at the band edge at $E_0=-65$ meV.

The experimental density of states $\rho_{2D}(x,E)$ in Fig. 3 can be analyzed in quantitative terms by a model where the step extends infinitely in the y direction, and represents a narrow

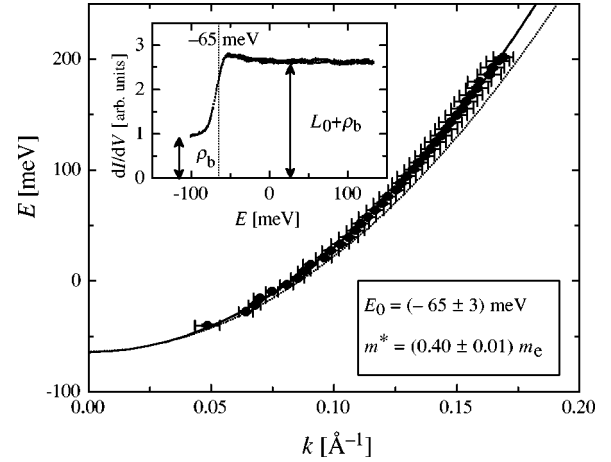


FIG. 4. Dispersion relation of the Ag(111) surface state. The solid line is a quadratic fit to our STM data and the dotted line shows results from photoemission data at 65 K (Ref. 3). The inset shows dI/dV data taken on a perfect terrace ($V=497$ mV, $I=5.0$ nA). The contribution of the surface LDOS to the measured total LDOS is $L_0/(\rho_{\text{bulk}}+L_0)\approx 0.64$.

potential barrier for surface-state electrons. We introduce the electronic wave function $\Psi_{E,k_y}(x,y)$, where $E=(\hbar^2/2m^*)(k_x^2+k_y^2)$ is the energy above E_0 , k_y , and k_x are the wave numbers parallel and perpendicular to the step, and m^* is the effective mass of the surface state electrons. Scattering of a plane wave at the step and its interference with the reflected wave are then described by $\Psi_{E,k_y}(x,y)=(e^{-ik_x x} + r e^{i\phi} e^{ik_x x}) e^{ik_y y}$, where r is the amplitude of the reflection and ϕ is the phase shift. The latter has been found to be $\phi = -\pi$ for Ag(111),¹⁵ which also holds for Cu(111). Following Davis *et al.*,²⁶ the LDOS of the 2D gas at a step is then given by

$$\rho_{2D}=L_0[1-rJ_0(2kx)], \quad (1)$$

where $L_0=m^*/(\pi\hbar^2)$, x is the distance from the step, $k^2=2m^*E/\hbar^2$, and J_0 is the zero-order Bessel function. The parameter r gives the amplitude of the *coherent* reflection at the step.

As seen in the lower graph of Fig. 3, constant energy cuts of the $dI/dV(E,x)$ plot can correctly be fitted with Eq. (1). By fitting $dI/dV(x)|_E$ at various energies, we obtain the wave number k for each energy, and thus the dispersion relation of the Ag(111) surface state. The result is displayed as $E(k)$ in Fig. 4. Our data are in excellent agreement with previously published results derived from STS (Ref. 9) and photoelectron spectroscopy (PES).³ The state is free-electron-like, the effective mass determined from a quadratic fit is $m^*=(0.40\pm 0.01)m_e$, and the band edge is located at $E_0=(-65\pm 3)$ meV with respect to E_F ($k_F=0.08$ \AA^{-1} , $\lambda_F=76$ \AA). In our experiments we have found no significant temperature dependence of $E(k)$ between 5 and 77 K. The inset of Fig. 4 shows dI/dV spectra taken on a wide terrace far from any scattering defect. The spectra show a steep increase in the LDOS at E_0 followed by a constant LDOS characteristic for a 2D free-electron gas; this measurement establishes the ratio $L_0/(\rho_{\text{bulk}}+L_0)$. The

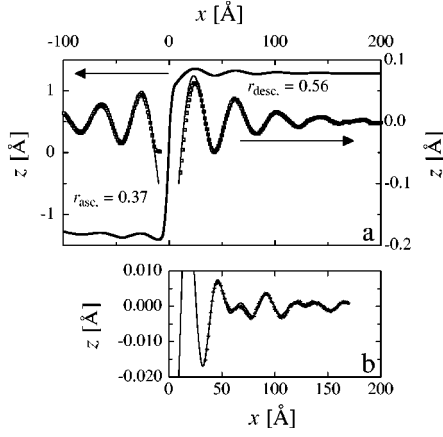


FIG. 5. Constant-current line scan taken across a Ag(111) step (a) at $V=10$ mV and $T=77.3$ K, and (b) at $V=100$ mV and $T=3.5$ K [$I=1.0$ nA in (a) and (b)]. The solid lines are fits using Eq. (4) (see text). The agreement between experiment and model is striking; also, pronounced beating effects appearing at large bias voltage as in (b) are perfectly reproduced. The only free fit parameters in (a) are the two reflection amplitudes $r_{\text{desc.}}$ and $r_{\text{asc.}}$ for descending and ascending steps.

contribution of surface state electrons to the LDOS detected by the STM is about twice that of electrons from bulk states.

B. Model for spatial damping

Our investigation of the spatial damping of standing waves is mostly based on constant-current line scans taken perpendicularly to steps at various sample temperatures. Such topographic data in the vicinity of a step are represented in Fig. 5. Although they are less directly related to the LDOS than dI/dV profiles, higher resolution can generally be obtained in topographic data. In Fig. 5, and also in the experimental results presented below, we averaged over several line scans which were recorded on the same surface spot, i.e., without y displacement of the tip while scanning in the x direction. Note the resolution of $\approx 1/1000$ Å of the $z(x)$ data presented in Fig. 5(b). We will now develop a model that relates the sample LDOS to constant-current line

scans, thus establishing the link of the decay of standing waves in the LDOS with the decay measured in topographic $z(x)|_{I,V}$ scans.

In elastic tunneling theory the tunneling current I is given by

$$I(eV, T, x, z) \propto \int_{-\infty}^{\infty} \mathcal{T}(E, eV, z) \rho_t(E - eV) \rho_s(E, x) \times [f(E - eV, T) - f(E, T)] dE, \quad (2)$$

where E is the energy measured with respect to the Fermi energy, ρ_s and ρ_t are the LDOS of the sample and tip, respectively, $\mathcal{T}(E, eV, z)$ is the transmission factor, and f is the Fermi-Dirac function ($e > 0$ in our convention). We make the assumption of a constant ρ_t . This is a good approximation at low bias since our dI/dV spectra correctly reproduce the constant LDOS for the 2D surface state (Fig. 4). The transmission factor is given by $\mathcal{T}(E, eV, z) = \exp[-(2z\sqrt{2m/\hbar})\sqrt{(\Phi_s + \Phi_t + eV)/2 - E}]$, where Φ_s and Φ_t are the respective work functions of the sample and tip. Numerical solution of the integral in Eq. (2) with parameters in the range of those used in our experiment yield that we can approximate the transmission factor by $\mathcal{T}(z) = \exp[-(1.025/\sqrt{eV\text{Å}})z\sqrt{\bar{\Phi}}]$, with $\bar{\Phi}$ representing the apparent barrier height.²⁷ This is a good approximation for x far enough from the step, where the barrier height is not influenced by the step. By ramping z and measuring the tunneling current I , we have determined $\bar{\Phi} = (3.1 \pm 0.1)$ eV.

Following Adawi,²⁸ the temperature effect in the integrand of Eq. (2) can be approximated by performing the integration at $T=0$ K and by multiplying the oscillating part of the resulting function with $\xi_k/\sinh \xi_k$, where

$$\xi_k = x \frac{2\pi m^* k_B T}{\hbar^2 k}. \quad (3)$$

Again, numerical solution of the integral in Eq. (2) shows that this procedure is very accurate. Thus we can readily calculate a very accurate *analytical* expression for the current $I(eV, T, x, z)$ in Eq. (2) perpendicular to a step by inserting ρ_s at a step: $\rho_s(E, x) = \rho_{2D}(E, x) + \rho_{\text{bulk}}$ and using Eq. (1) for ρ_{2D} . The result expressed for the tip height reads

$$z(x)|_{I,V} = \frac{\sqrt{eV\text{Å}}}{1.025\sqrt{\bar{\Phi}}} \ln \left[1 - r \frac{1}{eV} \frac{L_0}{\rho_{\text{bulk}} + L_0} \frac{\hbar^2}{2m^*} \frac{1}{x} e^{-2x/L_\phi} \left(\frac{\xi_k}{\sinh \xi_k} k J_1(2kx) - \frac{\xi_{k_F}}{\sinh \xi_{k_F}} k_F J_1(2k_F x) \right) \right] + \text{const}, \quad (4)$$

where $k(E) = \sqrt{(2m^*/\hbar^2)(eV - E_0)}$ is the wave vector at $E = eV$ with respect to E_F , and J_1 the first-order Bessel function. The oscillating term in Eq. (4) is due to coherence. Incoherent processes like electron-phonon or electron-electron scattering decrease its amplitude by the factor $\exp(-2x/L_\phi)$, where L_ϕ is the inelastic mean free path.²⁹ The distance from the step x appears twice, since in a scattering picture¹³ the electron has to travel forth to the step and back again to the STM tip.

According to Eq. (4), the damping of quantum interfer-

ence patterns as measured with STM is caused by a combination of inelastic scattering processes, Fermi-Dirac broadening, and beating between k_F and $k(E)$. To compare the damping strength of these different contributions we define, in addition to $L_\phi/2$ for inelastic processes, the following apparent coherence lengths. The expression of Fermi-Dirac (FD) broadening $\xi_k/\sinh \xi_k$ takes on the value $1/e$ at $\xi \approx 2.7$, and this defines $L_{\text{FD}} \approx 2.7(\hbar^2/2\pi m^*)(k/k_B T)$ [see Eq. (3)]. The beating of the Bessel functions $J_1(2kx)$ and $J_1(2k_F x)$ leads to a damping that attains the value $1/e$ at $L_{\Delta V} \approx 1/\Delta k$

with $\Delta k = k(eV) - k_F = \sqrt{2m^*/\hbar}(\sqrt{eV - E_0} - \sqrt{-E_0})$, or for small V , $\Delta k = m^*eV/\hbar^2 k_F$. Depending on the chosen conditions (V, T), one of these three damping lengths is shortest and dominates the decay.

To demonstrate the validity of our model, in Fig. 5(a) we present the fit by Eq. (4) to a topographic line scan taken across a monoatomic Ag(111) step. For Ag(111) the electron wave vector $k(E)$ and m^* are known from the dispersion relation and the ratio $L_0/(\rho_{\text{bulk}} + L_0) = 0.64$ has been estimated from dI/dV data on a clean terrace (see the inset of Fig. 4). Except from the reflection amplitudes $r_{\text{desc.}}$ and $r_{\text{asc.}}$ for the descending and ascending sides of the step, respectively, and the phase coherence length L_ϕ , all parameters entering Eq. (4) are known. The good agreement between model and experiment is evident. From our fit, which was performed with $L_\phi = \infty$ (see below), we obtain quite different reflection amplitudes r on the upper and lower terraces. For electrons reflected by the ascending step, $r_{\text{asc.}}$ is 1.8 ± 0.4 times smaller than for those approaching a descending step. The numerical values found here for $r_{\text{desc.}}$ and $r_{\text{asc.}}$ are fully confirmed by an experiment, where the LDOS is measured in Fabry-Pérot etalons built by parallel Ag(111) steps.¹⁵ The only free parameter in Eq. (4) is thus L_ϕ . For the data shown in Fig. 5(a) the dominant damping is due to L_{FD} .

The line scan in Fig. 5(b) was taken at a bias voltage of 100 mV. At these conditions $L_{\Delta V}$ prevails. The line scan shows the beating of the Bessel functions at $k_{100 \text{ meV}}$ and k_F . The beating and the amplitudes in $z(x)$ down to $1/1000 \text{ \AA}$ are perfectly described by Eq. (4).

C. Spatial damping on Ag(111)

In Fig. 6(a) we present line scans taken at $V = 10 \text{ mV}$ from 3.5 to 77.3 K on a Ag(111) terrace adjacent to a descending step. The damping of the standing waves with increasing T is clearly visible. The spatial damping of the electron standing waves in Fig. 6(a) for $x \geq 30 \text{ \AA}$ has been fitted by Eq. (4) by putting $L_\phi = \infty$. The data and the fitted function coincide almost perfectly, except in the immediate vicinity of the step edge where the model is not valid. The spatial damping is dominated by L_{FD} at high T , and by $L_{\Delta V}$ at low temperatures. It is clear from the fits that $L_\phi/2 > L_{\text{FD}}, L_{\Delta V}$ in the experiment. The only fit parameter $r_{\text{desc.}} = 0.56 \pm 0.06$ does not vary significantly with temperature.

Since the effective damping length L_{FD} due to Fermi-Dirac broadening is inversely proportional to T , at temperatures larger than 100 K, constant-current line scans taken at low bias voltage across a Ag(111) step show too few oscillations for a significant fit procedure. However, since $L_{\text{FD}} \propto k$ this problem can be circumvented by measuring quantities like dI/dV or dz/dV with lock-in techniques at larger bias (100 mV–1.5 V), or larger k , respectively. Figure 6(b) shows dI/dV data taken across a step at $T = 126 \text{ K}$. Taking into account the lock-in (modulation used for the measurement, these data are as well perfectly described by the theory.

Within our model the temperature-dependent damping of the standing waves is very well described by the Fermi-Dirac broadening alone. Therefore, we can only give lower limits for the phase-relaxation length L_ϕ . For Ag(111) surface-state electrons, L_ϕ is estimated to be $L_\phi(E_F) \geq 600 \text{ \AA}$ at 3.5

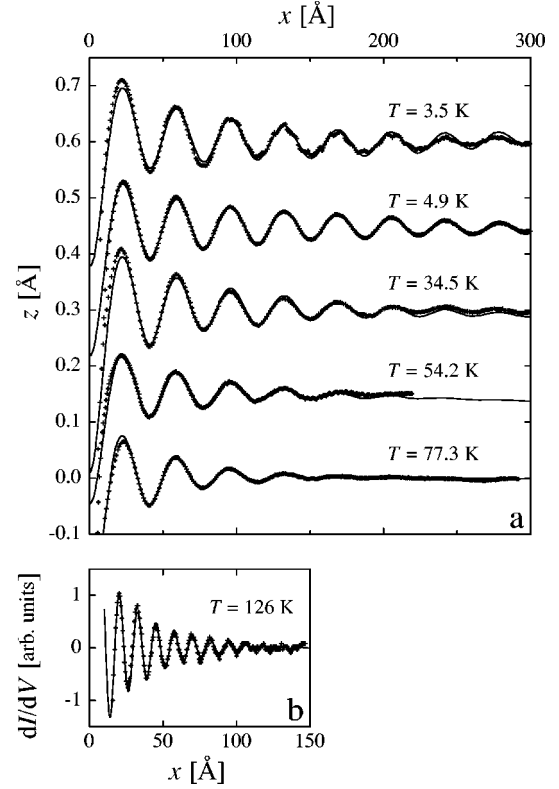


FIG. 6. (a) Ag(111) constant-current line scans taken on a terrace adjacent to a descending step ($V = 10 \text{ mV}$, $I = 1.0 \text{ nA}$). The data have been displaced vertically for clarity. (b) dI/dV data taken across a step at $V = 403 \text{ mV}$, $I = 4.3 \text{ nA}$, and $T = 126 \text{ K}$. The solid lines are fits using Eq. (4) in (a), and the according equation for dI/dV in (b), with the reflectivity r being the only fit parameter (L_ϕ was set to infinity; see text).

K and $L_\phi(E_F) \geq 250 \text{ \AA}$ at 77 K (see discussion for more details). These limits are obtained by reducing L_ϕ in the fit function [Eq. (4)], until a significant deviation from the experimental data is observed.

D. Spatial damping on Cu(111)

The Cu(111) surface state at $\bar{\Gamma}$ has been extensively studied by photoemission.^{1,2,10} It has a low-lying band edge of $E_0 = -0.44 \pm 0.01 \text{ eV}$ and an effective electron mass of $m^* = (0.38 \pm 0.02)m_e$ (Ref. 5) which is approximately the value determined above for Ag(111). Therefore, k_F is larger than for Ag(111) and with it also $L_{\text{FD}}(E_F)$ for a given temperature. At the Fermi energy Fermi-Dirac broadening is hence expected to play a smaller role for Cu(111) than for Ag(111). This explains why standing waves can be observed in constant current images on Cu(111) up to room temperature.³² Beating effects should also be smaller for Cu(111) due to its steeper dispersion in the vicinity of E_F . Despite the smaller STM intrinsic damping, inelastic scattering effects still remain small. Our results of the temperature induced spatial damping on the Cu(111) surface represented in Fig. 7 are, as for Ag(111), fully reproduced by Eq. (4) assuming $L_\phi = \infty$. Again, there is perfect agreement between model and experiment, and the observed apparent coherence loss can entirely be explained in the framework of Fermi-Dirac broadening and small beating effects. As in the case of

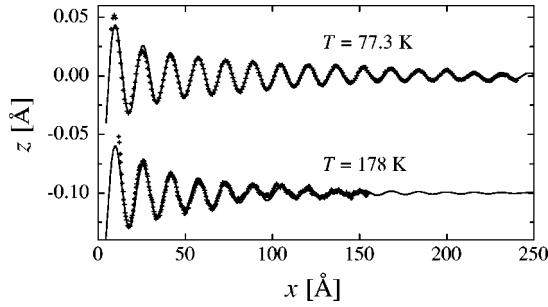


FIG. 7. Cu(111) constant-current line scans taken at $V = 10$ mV on a terrace adjacent to a descending step. The data have been displaced vertically for clarity ($I = 0.4$ nA at 77.3 K, $I = 0.1$ nA at 178 K). The solid lines are fits using Eq. (4) (L_ϕ was set to infinity; see text).

Ag(111) the lower limits of L_ϕ for Cu(111) are obtained by reducing L_ϕ in the fit function [Eq. (4)] until a significant deviation from the data is observed. The estimates are $L_\phi(E_F) \approx 660$ Å at 77 K and ≈ 160 Å at 178 K (see Fig. 8).

E. Discussion

Photoemission lines originating from surface states are preferred candidates for electron lifetime studies since surface states have no dispersion with respect to \mathbf{k}_\perp . Hence the instrumental final-state uncertainty in that quantity does not lead to broadening, and the linewidth Γ gives direct access to the lifetime broadening of the initial state. The currently most accurate photoemission studies of surface-state linewidths have been reported in Refs. 10 and 20 for Cu(111), and in Ref. 3 for Ag(111). From the T dependence of Γ , the

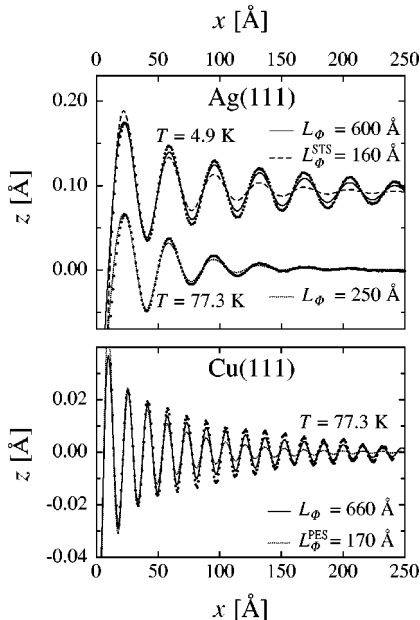


FIG. 8. Decay of standing waves as determined in experiment for Ag(111) and Cu(111) compared to results from Eq. (4) employing various values for the phase coherence length L_ϕ . It is clearly seen that the values deduced in former STS and PES studies are too small compared to our experimental result. (For a detailed discussion of, and references to L_ϕ^{STS} and L_ϕ^{PES} , see the text.)

authors of Ref. 10 derived the electron-phonon interaction strength of the $\bar{\Gamma}$ surface state on Cu(111). This quantity depends on the electron-phonon mass enhancement parameter λ . At elevated temperatures $k_B T > \hbar \omega_{\text{Debye}}$ there is the linear relationship $\Gamma_{e\text{-ph}} = 2\pi\lambda k_B T$. The result of $\lambda = 0.14 \pm 0.02$ was experimentally confirmed in Ref. 20, and agrees well with theory ($\lambda = 0.15 \pm 0.03$).³³ Despite the remarkable success of high-resolution photoemission to infer λ from $d\Gamma/dT$, the *absolute linewidths* Γ reported so far are all far above the theoretical predictions. This deficiency of PES is well known; it could be attributed to broadening by scattering at substrate imperfections.^{20,30,34} In agreement with this interpretation, Li *et al.* in a recent STS study on Ag(111) reported an unprecedented small Γ value from local measurements on surface areas that were bare of defects.³¹

In Fig. 8 we compare inverse lifetimes derived from STS and ARPES with our measurements of the decay of standing waves. For the sake of comparison we converted all quantities in $L_\phi = v_F \tau = v_F \hbar / \Gamma$, where v_F is the group velocity of the electrons at our measuring energy E_F . From the width of the onset of the Ag(111) surface state in tunneling spectra taken at 5 K, Li *et al.* derived $\tau(\bar{\Gamma}) = 67 \pm 8$ fs corresponding to $L_\phi^{\text{STS}} = v_F \tau(\bar{\Gamma}) \approx 160$ Å.³¹ It is evident from Fig. 8 that this result gives too large decay rates as compared to our Ag(111) data taken at E_F and 4.9 K. The shorter lifetime observed at $\bar{\Gamma}$ is probably partly due to the fact that the electron-phonon linewidth levels off at low temperature at the $\bar{\Gamma}$ point,¹⁰ and partly due to electron-electron interaction, which of course is enhanced at the $\bar{\Gamma}$ point as compared to E_F . It is also seen that our lower bound of $L_\phi(E_F) = 600$ Å is conservative; presumably $L_\phi(E_F)$ is much larger. Our L_ϕ value presents the largest lifetime measured so far for the Ag(111) surface state. It corresponds to a peak width of $\Gamma(E_F, 5 \text{ K}) = (\hbar^2 k_F / m^* L_\phi) \leq 2.6$ meV, which should be very difficult to resolve in ARPES.

In a Debye model the phase relaxation length due to electron-phonon interaction close to E_F is well described by $L_\phi(E_F, T) = (v_F \hbar / 2\pi\lambda k_B T)$ for $k_B T \geq \hbar \omega_{\text{Debye}}$.^{10,33} At lower temperatures L_ϕ lies below this asymptotic limit and can be evaluated by a simple numerical integration, with λ being the only free parameter.^{10,33} In both cases an absolute measurement of $L_\phi(E_F)$ at a single T yields an estimate of λ . We used the Debye model of Ref. 10 to derive such estimates from our $L_\phi(E_F)$ values. For Ag ($\hbar \omega_D^{\text{Ag}} = 19$ meV) we derive $\lambda_{\text{Ag}} \leq 0.27$ from $L_\phi(E_F, 77.3 \text{ K}) \approx 250$ Å. This conservative upper limit for the electron-phonon mass enhancement factor is in agreement with the bulk value of $\lambda_{\text{Ag}} = 0.13 \pm 0.04$ given by Grimwall.³³

The currently lowest intrinsic line width measured by PES for the $\bar{\Gamma}$ surface state on Cu(111) is $\Gamma(\bar{\Gamma}, 77 \text{ K}) = 36$ meV.¹⁰ By deducing the difference of electron-phonon and electron-electron linewidths between $\bar{\Gamma}$ and E_F of $\Delta\Gamma = 8$ meV + 5 meV = 13 meV (values inferred from the Debye model displayed for $\lambda = 0.14$ in Fig. 1 of Ref. 10), we estimate the resulting PES linewidth at E_F to be about $\Gamma(E_F, 77 \text{ K}) = 23$ meV, respectively, $L_\phi^{\text{PES}}(E_F, 77 \text{ K}) \approx 170$ Å. Figure 8 shows that this coherence length again is considerably too short compared to the observed decay

length of the standing waves. Our lower bound of $L_\phi(E_F, 77 \text{ K}) = 660 \text{ \AA}$ yields a linewidth of $\Gamma(E_F, 77 \text{ K}) = 6 \text{ meV}$. From this upper bound, and consistently from our measurement at 178 K [$\Gamma(E_F, 178 \text{ K}) \leq 26 \text{ meV}$], we derive an upper limit of $\lambda_{\text{Cu}} \leq 0.34$ with a Debye model¹⁰ using $\hbar \omega_D^{\text{Cu}} = 27 \text{ meV}$. Again this is a conservative estimate which is in accordance with $\lambda = 0.14$ measured with ARPES.

One evident reason why we measure much larger coherence lengths than can possibly be obtained with PES is that we determine L_ϕ locally at terrace stripes perpendicular to steps that are bare of any adsorbates or other steps on the length scale of L_ϕ . From large-scale observations of the surface morphology it is clear, however, that most crystals present surface areas where the average terrace width is below our L_ϕ values. Also the density of chemical defects is often above $1/L_\phi^2$ for L_ϕ in the range discussed here. Every integrating technique will be embarrassed by the steps and point defects since surface-state electrons strongly couple to the bulk at these sites.¹⁵ This leads to an apparent reduction of the integral L_ϕ as seen in PES. We therefore believe that the ‘‘offset’’ of $\Gamma(0 \text{ K}) \approx 20\text{--}30 \text{ meV}$ characterizing high-resolution PES peaks is mainly due to structural defects such as steps. This assignment is supported by differences of up to 10 meV in the linewidth ‘‘offset’’ between different research groups, whereas there is good agreement on $d\Gamma/dT$.^{10,20} The influence of sputter defects on the linewidth Γ was employed to extrapolate to ‘‘intrinsic’’ linewidths expected from PES of perfectly ordered surfaces.³⁰ The resulting ‘‘intrinsic’’ values, e.g., of $\Gamma(\bar{\Gamma}, 0 \text{ K}) \leq 21 \pm 5 \text{ meV}$ for Cu(111), still contain phonon excitation at 0 K and electron-electron interactions.

The alternative approach to look at STS peak widths eliminates the defect problem; however, an analysis in terms of lifetimes demands elaborate modeling. We note that our STS peak widths (see Fig. 4) are comparable to the ones reported by Li *et al.*,³¹ hence we would infer similar estimates on τ from regarding $\Gamma(\bar{\Gamma}, 5 \text{ K})$ in our STS spectra. Compared to a peak width analysis, our access to τ via measuring L_ϕ from the decay of standing waves has two advan-

tages: (i) it is based on a straightforward analytical model that has been tested experimentally (see Sec. III B); and (ii) since we measure at E_F , our L_ϕ values are not reduced by electron-electron interaction or phonon excitation at 0 K, and therefore provide a more direct access to λ . With our method to measure lifetimes of surface-state electrons via the decay length L_ϕ of quantum-mechanical interference patterns, we can freely choose the electron energy (in dI/dV). Our lower bounds of $L_\phi(E_F)$ approach the theoretical limits of lifetimes of surface-state electrons.

IV. CONCLUSIONS

In conclusion, the quantum interference of surface-state electrons near monoatomic steps on Ag(111) and Cu(111) has been studied in the temperature range of 3.5–178 K. We derived the dispersion of the surface state $E(k)$ for Ag(111), and found no significant temperature dependence of E_0 and m^* in the range up to 77 K. The temperature-dependent spatial damping of constant-current line scans and dI/dV data at steps are perfectly explained by elastic tunneling theory. Thus the phase-relaxation length $L_\phi(E_F)$ of 2D electrons is larger than the damping length L_{FD} due to the Fermi broadening of the STM beam. Nevertheless, we were able to derive lower bounds for $L_\phi(E_F, T)$ pointing to significantly longer lifetimes than all data currently available for surface states. In the case of high-resolution photoemission there is a residual linewidth due to defects such as steps. This effect is absent in our measurement as we evaluate the standing waves at surface spots which are bare of defects within the range of L_ϕ . Inelastic electron-electron scattering is avoided by measuring close to E_F . In contrast to studies of the energetic peak width of the surface state we directly estimate L_ϕ , and the lifetime τ , respectively, and our estimates point toward infinite values at 4 K. We can derive estimates for the electron-phonon mass enhancement factor from $L_\phi(E_F, T)$ measured for a single $T \neq 0$. Our absolute values of L_ϕ can be combined with high-resolution PES data to derive an accurate description of $L_\phi(T)$.

¹P. O. Gartland and B. J. Slagsvold, Phys. Rev. B **12**, 4047 (1975).
²S. D. Kevan, Phys. Rev. Lett. **50**, 526 (1983).
³R. Panagio, R. Matzdorf, G. Meister, and A. Goldmann, Surf. Sci. **336**, 113 (1995).
⁴J. Friedel, Nuovo Cimento **7**, 287 (1958); J. Phys. Radium **19**, 38 (1958).
⁵M. F. Crommie, C. P. Lutz, and D. M. Eigler, Nature (London) **363**, 524 (1993).
⁶Y. Hasegawa and P. Avouris, Phys. Rev. Lett. **71**, 1071 (1993).
⁷M. F. Crommie, C. P. Lutz, and D. M. Eigler, Science **262**, 218 (1993).
⁸G. Hörmandinger, Phys. Rev. B **49**, 13 897 (1994).
⁹J. Li, W.-D. Schneider, and R. Berndt, Phys. Rev. B **56**, 7656 (1997).
¹⁰B. A. McDougall, T. Balasubramanian, and E. Jensen, Phys. Rev. B **51**, 13 891 (1995).
¹¹L. Petersen, P. T. Sprunger, Ph. Hofmann, E. Laegsgaard, B. G.

Briner, M. Doering, H. P. Rust, A. M. Bradshaw, F. Besenbacher, and E. W. Plummer, Phys. Rev. B **57**, R6858 (1998).
¹²P. Avouris and I. W. Lyo, Science **264**, 942 (1994).
¹³E. J. Heller, M. F. Crommie, C. P. Lutz, and D. M. Eigler, Nature (London) **369**, 464 (1994).
¹⁴J. Li, W.-D. Schneider, R. Berndt, and S. Crampin, Phys. Rev. Lett. **80**, 3332 (1998).
¹⁵L. Bürgi, O. Jeandupeux, A. Hirstein, H. Brune, and K. Kern, Phys. Rev. Lett. **81**, 5370 (1998).
¹⁶P. Avouris, I. W. Lyo, R. E. Walkup, and Y. Hasegawa, J. Vac. Sci. Technol. B **12**, 1447 (1994).
¹⁷S. Datta, *Electronic Transport in Mesoscopic Systems* (Cambridge University Press, Cambridge, 1995).
¹⁸K. K. Choi, D. C. Tsui, and K. Alavi, Phys. Rev. B **36**, 7751 (1987).
¹⁹G. Dumpich and A. Carl, Phys. Rev. B **43**, 12 074 (1991).
²⁰R. Matzdorf, G. Meister, and A. Goldmann, Phys. Rev. B **54**, 14 807 (1996).

- ²¹R. Matzdorf, Surf. Sci. Rep. **30**, 153 (1998).
- ²²A. Goldmann, R. Matzdorf, and F. Theilmann, Surf. Sci. **414**, L932 (1998).
- ²³H. Brune, Surf. Sci. Rep. **31**, 121 (1998).
- ²⁴J. Frohn, J. F. Wolf, K. Besocke, and M. Teske, Rev. Sci. Instrum. **60**, 1200 (1989).
- ²⁵K. Besocke, Surf. Sci. **181**, 145 (1987).
- ²⁶L. C. Davis, M. P. Everson, R. C. Jaklevic, and W. Shen, Phys. Rev. B **43**, 3821 (1991).
- ²⁷L. Olesen, M. Brandbyge, M. R. Sørensen, K. W. Jacobsen, L. Laegsgaard, I. Stensgaard, and F. Besenbacher, Phys. Rev. Lett. **76**, 1485 (1996).
- ²⁸I. Adawi, Phys. Rev. **146**, 379 (1966).
- ²⁹L. Bürgi, H. Brune, and K. Kern, Phys. Rev. Lett. (to be published).
- ³⁰F. Theilmann, R. Matzdorf, G. Meister, and A. Goldmann, Phys. Rev. B **56**, 3632 (1997).
- ³¹J. Li, W.-D. Schneider, R. Berndt, O. R. Bryant, and S. Crampin, Phys. Rev. Lett. **81**, 4464 (1998).
- ³²E. Wahnström, I. Ekvall, H. Olin, and L. Walldén, Appl. Phys. A: Mater. Sci. Process. **66A**, S1107 (1998).
- ³³G. Grimvall, *The Electron-Phonon Interaction in Metals* (North-Holland, New York, 1981).
- ³⁴J. Tersoff and S. D. Kevan, Phys. Rev. B **28**, 4267 (1983).